Enhanced Skin Cancer Classification with MobileNetV3 and Morphological Preprocessing: A Deep Learning-Based Extension

Sidra Mehboob[1], Maryam Bukhari[1], Yaser Ali Shah[1], Salabat Khan[2], Muhammad Sharif[1]
[1]Department of Computer Science COMSATS University Islamabad, Attock Campus Attock 43600, Pakistan
DOI: https://doi.org/10.33411/IJIST/1349
[2]Big Data Research Center Jeju National University Jeju 63243, Republic of Korea
*Correspondence: Muhammad Sharif, m.sharif@cuiatk.edu.pk
Citation | Mehboob. S, Bukhari. M, Shah. Y. A, Khan. S, Sharif. M, "Enhanced Skin Cancer Classification with MobileNetV3 and Morphological Preprocessing: A Deep Learning-Based Extension", IJIST, Vol. 07 Special Issue. pp 1-12, May 2025
Received | April 10, 2025 **Revised |** April 29, 2025 **Accepted |** May 03, 2025 **Published |** May 04, 2025.

Skin cancer detection continues to pose challenges due to the visual similarity between the types of lesions and the limitations of traditional diagnostic methods. This study presents an extended and improved skin lesion classification framework that combines transfer learning with MobileNetV3 and enhanced preprocessing using mathematical morphological techniques. These preprocessing methods refine lesion boundaries and suppress irrelevant structures in dermoscopic images, thereby improving feature discrimination during training. The refined framework is evaluated using the ISIC dataset and achieves a notable classification accuracy of 89%, showing superior performance compared to baseline models. This extension also examines the generalizability and suitability of the model for deployment in low-resource mobile settings. The results validate the effectiveness of lightweight architectures paired with morphological enhancements, providing a reliable and scalable solution for early skin cancer screening and clinical support.

Keywords: Skin Cancer Detection, Transfer Learning, MobileNetV3, Mathematical Morphology, Dermoscopic Image Classification

Introduction:

Skin cancer is among the most prevalent and life-threatening forms of cancer globally. Early identification of skin lesions, particularly melanoma, plays a critical role in reducing mortality rates. With increasing exposure to ultraviolet (UV) radiation and lifestyle changes, the incidence of skin cancer has increased significantly over the past few decades. Countries such as the United States, Australia, and Canada have reported a steep increase in melanoma cases, especially among individuals aged 30 and older. In this context, computer-aided diagnostic (CAD) systems have become indispensable tools for helping dermatologists detect skin cancer through dermoscopic image analysis. These systems offer a noninvasive, efficient, and cost-effective approach to early diagnosis, which can greatly improve treatment outcomes.

Traditional machine learning (ML) methods were among the first solutions introduced to automate the detection of skin cancer. These approaches involve manual feature extraction techniques, in which texture, shape, color, and size are extracted and passed to classifiers such as SVM, KNN, or Naive Bayes [1][2][3][4][5][6][7][8]. Although these systems outperformed manual diagnostic accuracy, they required complex preprocessing and domain expertise for feature engineering. Techniques such as the Firefly algorithm with KNN [4], GLCM with SVM [5], and HOG with LDA [6] have shown promising results. However, these methods often struggle with variations in the appearance of the lesion and background noise, reducing their reliability in real-world applications.

With the advent of deep learning (DL), Convolutional Neural Networks (CNNs) began to replace traditional techniques due to their ability to perform automatic feature extraction. Pre-trained models such as AlexNet, ResNet50, Inception-V3, and VGG19 have demonstrated remarkable performance in classifying benign and malignant lesions [9][10][11][12][13][14]. Transfer learning further enhanced these architectures by enabling the reuse of learned features from large-scale datasets, which is particularly useful when domain-specific labeled data are limited. However, while CNNs reduce manual intervention, they still face issues related to low image contrast, noise, and ambiguous lesion boundaries that affect classification performance.

To address these shortcomings, researchers have explored ensemble learning, multi-model systems, and attention-based mechanisms. Ensemble strategies that combine the output of ResNet, DenseNet, VGG16, and Inception networks have shown superior accuracy, reaching up to 98.6% in some studies [15], [16]. Other innovations, such as IoHT-integrated CAD systems [12] and attention mechanisms [17], were aimed at improving feature discrimination. Furthermore, hybrid systems that combine deep learning feature extraction with traditional classifiers have been proposed [18]. However, most existing methods are either computationally intensive or not optimized for deployment in mobile and resource-limited environments.

Despite significant progress, current systems still face key limitations. Many deep learning models require high-end computing resources, making them unsuitable for real-time or mobile-based applications. In addition, some models fail to generalize well due to challenges such as varying lesion sizes, poor image quality, and class imbalance in datasets. This study aims to bridge these gaps by investigating the following research questions: (1) How can we optimize deep learning models for low-resource environments without compromising performance? (2) Can mathematical morphology improve dermoscopic image quality for improved classification?

The main objective is to develop an efficient, accurate, and lightweight CAD system capable of real-time skin cancer detection. To meet these objectives, we propose a novel framework that combines the MobileNetV3 architecture with mathematical morphology-based preprocessing techniques. MobileNetV3 is selected for its balance between accuracy and computational efficiency, making it ideal for mobile deployment. The preprocessing stage

enhances the features of the dermoscopic image, allowing the model to learn more effectively from the input data. Based on the ISIC dataset, our system achieves a classification accuracy of 89% and a recall of 85%, outperforming several existing models.

The contributions of this research are threefold: (1) design of a lightweight and accurate deep learning model, (2) enhancement of image quality using morphological operations, and (3) demonstration of a scalable solution for real-time skin cancer diagnosis. This work paves the way for future mobile health applications that support dermatologists and patients in timely and accurate diagnosis.

The rest of the paper is organized into various sections: The next section identifies the proposed approach in detail. The Result and Discussion section explains the experimental results, and the last section concludes the study with future directions.

Material and Methods:

In this section, we explain our suggested method in detail, step by step. The pictorial view of the suggested methodology is depicted in Figure. 1.

Preprocessing:

In the first stage, we applied preprocessing steps on dermoscopic images to remove noise and other artifacts so that the resulting images are enhanced and clearer in visibility. Therefore, we resized all images from the dataset to fixed dimensions of 224×224×3. Later, in all images, we applied the morphological operation, i.e., a dilation followed by the erosion operation. This operation removed the extra noise appearing on the dermoscopic images of skin cancer.

After that, the 2D kernel matrix was used to convolve the given dermoscopic image to enhance and improve the contrast of the image, as shown in Figure. 2. The kernel matrix is the sharpening kernel given below.

$$\text{Kernel} = \begin{matrix} 0 & -1 & 0 \\ -1 & 5 & -1 \\ 0 & -1 & 0 \end{matrix} \quad (1)$$

The equation above (1) shows the kernel matrix used to sharpen the image after going through morphological operations. All these preprocessing steps prepare the data to be given as input to the deep CNN model.

MobileNetV3 Architecture:

MobileNetV3 is a variant of the Convolutional Neural Network (CNN) architecture designed for mobile devices. The architecture is characterized by its use of depthwise separable convolutions, which help reduce computation and improve performance on resource-constrained devices. The general architecture of MobileNetV3 can be divided into three main building blocks. The initial block typically includes a single convolutional layer and a max pooling layer. The main body of the network is composed of several inverted residual blocks. Each block includes a depthwise separable convolution, a pointwise convolution, and an optional expansion layer. The final block includes a global average pooling layer and a fully connected layer for classification. The architecture diagram of MobileNetV3 is shown in Figure. 1

MobileNetV3 also includes two versions: MobileNetV3-Large, which is a larger, more powerful version of the architecture, and MobileNetV3-Small, which is a smaller, more efficient version. The main difference between these two versions is the number of channels in the inverted residual blocks and the number of blocks in the main body of the network.

Previously, MobileNet-based deep learning architectures have been introduced. In the first version, MobileNetV1 [19], depthwise separable convolutions were proposed, showing significant improvements over existing architectures. Later, MobileNetV2 [20] added the linear bottleneck and inverted residual modules to create more effective layer

structures by utilizing the low-rank characteristics of the data. However, in MobileNetV3, the authors developed the most efficient methods by employing a mix of efficient layers as key components, along with modified swish nonlinearities added to the layers [21][22][23].B. Transfer Learning using MobileNetV3.

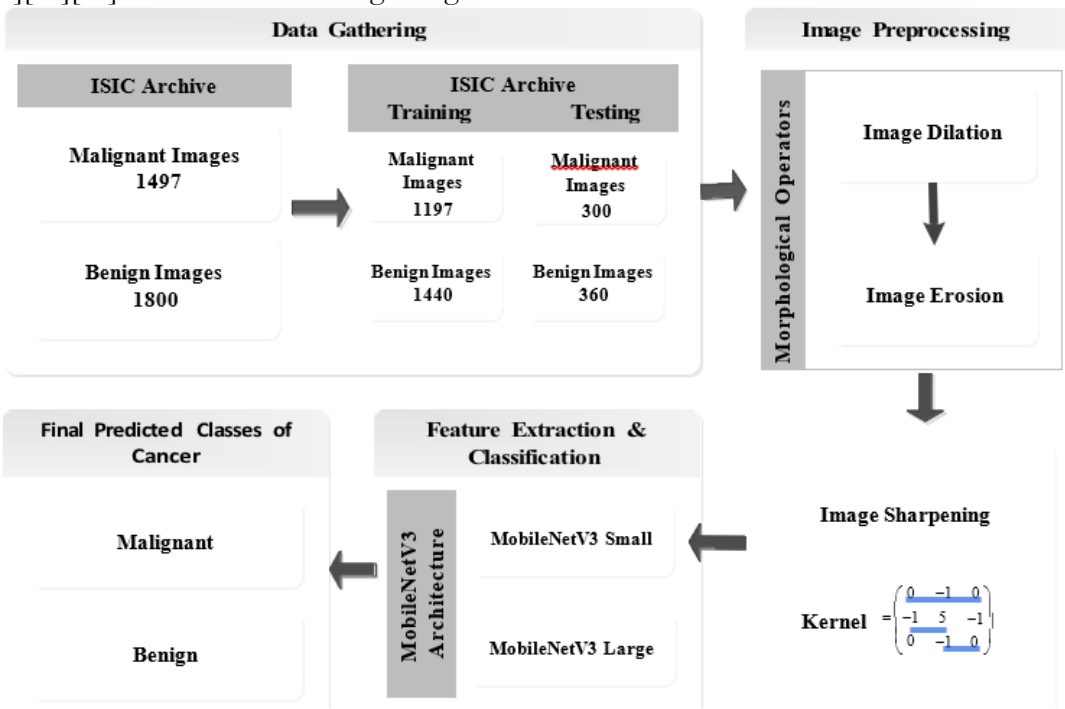


Figure 1. Process Flow Diagram of the Proposed Methodology.

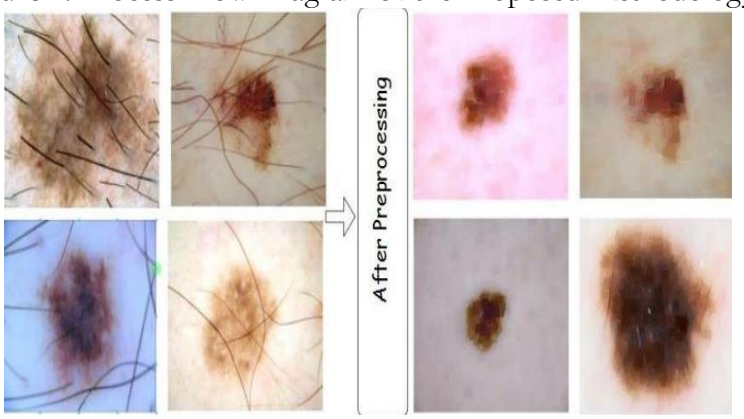


Figure 2. Results of Preprocessing Operations.

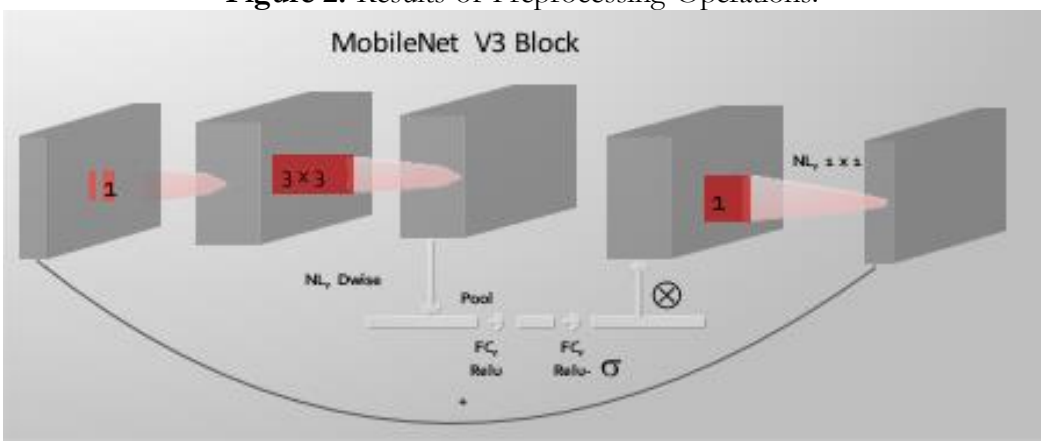


Figure 3. Architecture Diagram of MobileNetV3.

Despite having a significant number of trained images, the dataset is still not large enough to create a new deep-learning model from scratch. To tackle this challenge, the technique of transfer learning is applied to the pre-trained MobileNetV3 architecture due to its efficient feature learning capabilities. For this purpose, the pre-trained MobileNetV3 model [24] is initially loaded. This model was trained on the ImageNet dataset, one of the largest image classification datasets available.

Subsequently, the weights of the initial layers are frozen by setting their trainable parameters to false. After freezing the base layers, a flattening layer is added, followed by two fully connected (dense) layers. The first dense layer consists of 512 units with the 'ReLU' activation function. The final dense layer contains a single unit with the 'sigmoid' activation function to perform binary classification. Additionally, a dropout layer with a dropout rate of 0.25 is inserted between the two dense layers to help prevent overfitting. The loss function used for training is binary cross-entropy, as skin cancer classification (malignant vs. benign) is inherently a binary classification task. Table I provides the list of hyperparameters configured for the model.

MobileNetV3 is a highly efficient convolutional neural network designed for deployment on mobile devices and edge devices. It integrates techniques such as depthwise separable convolutions, squeeze-and-excitation blocks, and the hard-swish activation function, and employs neural architecture search to enhance both speed and accuracy. The development of this architecture stems from earlier versions: MobileNetV1, which introduced a lightweight design using depthwise separable convolutions to reduce complexity, and MobileNetV2, which refined performance through the use of inverted residuals and linear bottlenecks. MobileNetV3 advances these concepts by offering superior performance-to-efficiency ratios compared to its predecessors. In the context of this study, the use of MobileNetV3 as a classifier for skin cancer images is particularly beneficial, as it delivers accurate predictions while remaining computationally lightweight, making it ideal for early diagnosis through mobile or low-resource platforms.

The hyperparameter configuration described in Table I was fine-tuned to optimize the performance of the model for binary skin cancer classification. The Adam optimizer was used because of its adaptive learning rate and robust convergence properties, which are particularly beneficial for deep-learning tasks involving medical images. A small learning rate of 0.00001 was chosen to ensure gradual and stable weight updates, reducing the risk of overshooting minima during training. A batch size of 4 was used to accommodate memory limitations and maintain model generalization. Binary cross-entropy was selected as the loss function, aligning with the binary nature of the classification task. To mitigate overfitting, a dropout rate of 0.25 was applied, randomly deactivating a portion of neurons during training. The ReLU activation function was used in the hidden layers for its efficiency and ability to handle nonlinearity, while the sigmoid function in the output layer was appropriate for generating probability scores in binary classification. The model was trained for 25 epochs, which offered a balance between sufficient learning and avoiding overfitting, based on validation performance. This hyperparameter setup played a critical role in enhancing both the robustness and predictive accuracy of the proposed classification framework.

Dataset:

In this research study, a publicly available skin cancer image dataset from Kaggle was utilized, containing two categories: malignant and benign. The dataset consists of a total of 3,297 images, organized into separate training and testing folders. These images were originally sourced from the ISIC archive, a well-known repository for skin cancer research. The distribution of images — including the number of malignant and benign samples in both the training and testing sets — is detailed in Table I.

Table 1. Data Distribution for Experiments

Class	Train	Test	Total
Malignant	1197	300	1497
Benign	1197	300	1497
Total	**2637**	**660**	**3297**

Performance Metrics:

The following performance analysis criteria were used to evaluate the model's effectiveness: accuracy, precision, recall, F1-score, confusion matrices, and ROC curves. Accuracy, one of the most commonly used metrics, assesses the overall correctness of the model. However, in cases where the dataset is imbalanced, additional metrics such as precision and recall become crucial. Precision measures the model's ability to correctly identify positive instances, whereas recall evaluates its ability to capture all actual positive instances. A higher recall value indicates better performance in detecting the positive class. The F1-score provides a harmonic mean between precision and recall, offering a balanced evaluation metric. Additionally, the confusion matrix presents a detailed summary of classification results in a compact form. Finally, ROC curves are plotted to further assess the model's diagnostic ability across different thresholds. The mathematical expressions for the performance metrics — accuracy (Eq. 2), precision (Eq. 3), recall (Eq. 4), and F1-score (Eq. 5) — are provided below.

$$Accuracy = \frac{TP+TN}{TP+TN+FP+FN} \times 100\% \quad (1)$$

$$Precision = \frac{TP}{TP+FP} \times 100\% \ (2)$$

$$Recall = \frac{TP}{TP+FN} \times 100\% \ (3)$$

$$F1-Score = 2 \times \frac{Precision \times Recall}{Precision + Recall} \times 100\% \quad (4)$$

Where TP, TN, FP, and FN denote True Positive, True Negative, False Positive, and False Negative, respectively.

The list of Hyperparameter settings is shown in Table 2.

Results And Discussions:

In this section, the results obtained from the designed model are presented.

Table 2. List of Hyperparameter Settings

Parameter	Value
Weight Optimizer	Adam
Learning Rate	0.00001
Batch Size	4
Loss Function	Binary Cross-Entropy
Dropout Ratio	0.25
Activation Function (Hidden Layer)	ReLU
Activation Function (Output Layer)	Sigmoid
Epochs	25

Performance Analysis of the Proposed Framework:

In this section, the effectiveness of the proposed algorithm is evaluated after applying the preprocessing steps. The results of the preprocessing phase are illustrated in Figure. 2. Initially, the model is trained using the training set, which includes images classified as malignant and benign.

For the MobileNetV3-Large model, the results in the malignant class achieved an accuracy of 89%, precision of 92%, recall of 87%, and an F1-score of 89%. In the benign class, the corresponding values are 89% for accuracy, 85% for precision, 91% for recall, and 88% for F1-score. The overall accuracy achieved in this experiment using the Adam optimizer is 89%.

In comparison, for the MobileNetV3-Small model, the accuracy, precision, recall, and F1-score in the malignant class are 87%, 88%, 87%, and 88%, respectively. In the benign class, these values are 87% for accuracy, 85% for precision, 86% for recall, and 86% for F1-score.

From the overall experimental results, it can be concluded that the MobileNetV3-Large model outperforms the MobileNetV3-Small model in terms of average accuracy and general performance across both classes.

Table 3 Confusion Matrix of the Proposed Methodologies

Metric	MobileNetV3 Small with Mathematical Morphology	MobileNetV3 Large with Mathematical Morphology
True Positive	260	275
True Negative	315	314
False Positive	45	46
False Negative	40	25

Table 4. Results of MobileNetV3-Large

Class	Accuracy	Precision	Recall	F_1-Score
Malignant	89%	92%	87%	89%
Benign	89%	85%	91%	88%

Table 5. Results of MobileNetV3-Small

Class	Accuracy	Precision	Recall	F_1-Score
Malignant	87%	88%	87%	88%
Benign	87%	85%	86%	86%

Table III shows the confusion matrix using the Mo- bileNetV3 Small and Large with mathematical morphology. In the case of the MobileNetV3-Large model, 314 samples of the malignant class and 275 samples of the benign class were correctly classified from the overall test set. However, 46 malignant and **25** benign samples were misclassified.

More precisely, we individually assessed the performance of the proposed MobileNetV3 framework across both skin cancer classes—malignant and benign. The detailed performance metrics, including accuracy, precision, recall, and F1-score for each class, are provided in **Tables IV and V**.

Additionally, the training accuracy and loss values were recorded epoch by epoch, as illustrated in Figure. 6. From the graph, it can be observed that the training accuracy remains high when using the Adam optimizer. Similarly, the second graph displays the loss values, where it is evident that the training loss decreases consistently with the Adam optimizer, aligning with the trends observed in the accuracy graph.

Furthermore, when evaluating the proposed model's performance on the test set, it is clear that the accuracy values are higher when optimized with Adam. In summary, the individual effectiveness of the algorithm for both malignant and benign classes has been thoroughly analyzed, demonstrating the robustness of the proposed MobileNetV3-Large framework.

The ROC curve is primarily employed to analyze the categorization model's efficacy. It plots the relationship between true positive rates and false positive rates, providing a comprehensive visualization of the model's performance. Furthermore, during training, the model exhibits high training accuracy values and very low loss values, indicating effective learning.

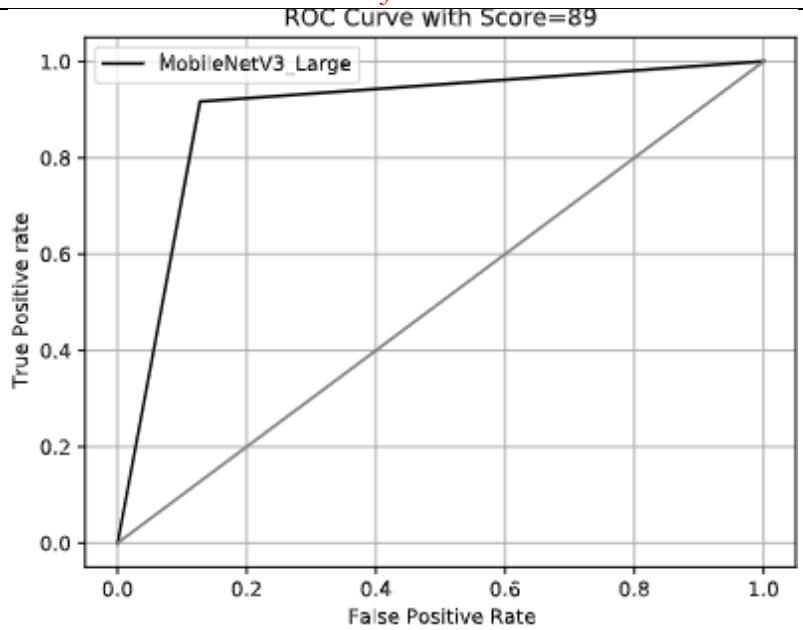


Figure 4. ROC Curve generated by MobileNetV3 Large with Mathematical Morphology.

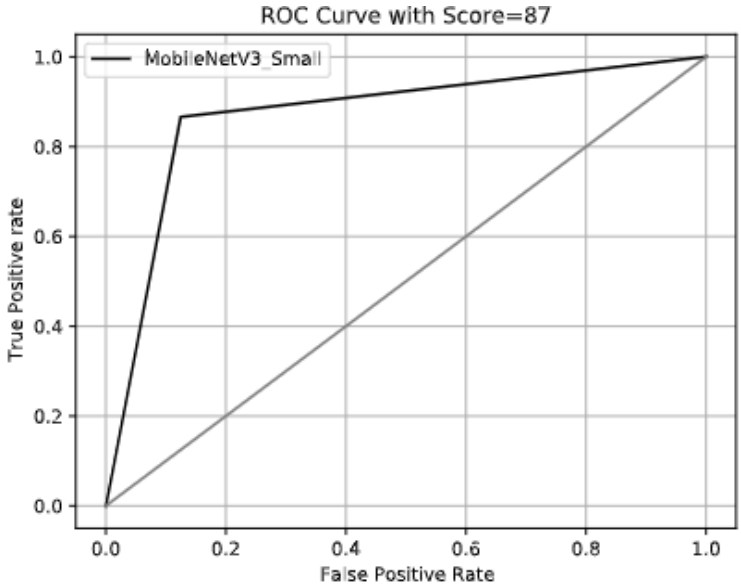


Figure 5. ROC Curve generated by MobileNetV3 Small with Mathematical Morphology.

Discussion:

It is observed from the above-presented results and Table 5, that the designed framework shows the best results in terms of accuracy, precision, recall, and F1 Score values. The comparison is done only on those approaches that have used the same dataset. Further, in an attempt to discuss the suggested model's evaluation, the results of the proposed technique are compared with existing methods. For instance, Manasa et al. [25] suggest the Vgg16-based deep learning model and have achieved an 86.6% accuracy. Similarly, Bechlli et al. [26] combined the three pre-trained models, namely VGG16, ResNet50, and DenseNet, as an ensemble network and achieved 85% accuracy.

Our proposed model shows an accuracy of 87% and 89% with MobileNetV3Small and MobileNetV3Large versions, respectively. The comparison of the proposed and existing techniques is tabulated in Table VI.

Although the proposed skin cancer classification framework shows promising performance, several challenges and limitations need to be considered. One of the primary

concerns is the potential for overfitting, particularly given the relatively small dataset. Despite implementing regularization techniques such as dropout, the model may still overfit to specific patterns in the training data, hindering its ability to generalize effectively to unseen examples. Furthermore, data imbalance is a common issue in medical imaging datasets, where the distribution of malignant and benign cases may not be equal. This imbalance could lead to bias in the model predictions, potentially promising the detection of less prevalent cases of skin cancer. The small size of the dataset further exacerbates these issues, as the model may not be exposed to a sufficiently diverse range of types of lesions and imaging conditions, which affects its robustness in practical deployment. To mitigate these challenges, future work should consider utilizing larger, more diverse datasets, along with advanced techniques like data augmentation or re-sampling, to enhance model generalization and overall performance.

Conclusion:

Skin cancer remains one of the deadliest diseases worldwide. The color images of skin lesions often show a significant degree of resemblance between different types, such as malignant and benign, making accurate identification and diagnosis particularly challenging. Timely detection is crucial and requires a reliable automated process for categorizing skin cancer, ultimately saving time, effort, and lives.

In this research article, an attempt was made to provide a deep learning-assisted solution based on a transfer learning approach using the MobileNetV3 model. MobileNetV3 is chosen for its enhanced feature learning capabilities, owing to the specialized design of its layers. In addition to the classification results, ROC curves were plotted, as shown in Figures 4 and 5, for both MobileNetV3-Small and MobileNetV3-Large models, further validating the model's performance. The Receiver Operating Characteristic (ROC) curve helps in visualizing the trade-off between true positive and false positive rates, highlighting the robustness of the framework. Overall, the proposed framework demonstrates effective performance, achieving high values of accuracy, precision, recall, and F1-Score, confirming its reliability for skin cancer classification tasks. The findings suggest that this strategy may be an acceptable way to diagnose skin cancer early and accurately, providing a practical tool that can be used in real-time on mobile devices.

TABLE 6. Comparison of the Proposed and Existing Technique.

Research paper [reference]	Approach	Accuracy
Manasa et al. [23]	VGGA16	86%
Bechelli et al. [26]	VGG16, Xception, ResNet50	85%
Demir et al. [25]	ResNet-101	84.09%
Demir et al. [25]	Inception-V3	87.42%
Proposed	MobileNetV3 Small	87%
Proposed	MobileNetV3 Large	89%
Proposed	Average	88%

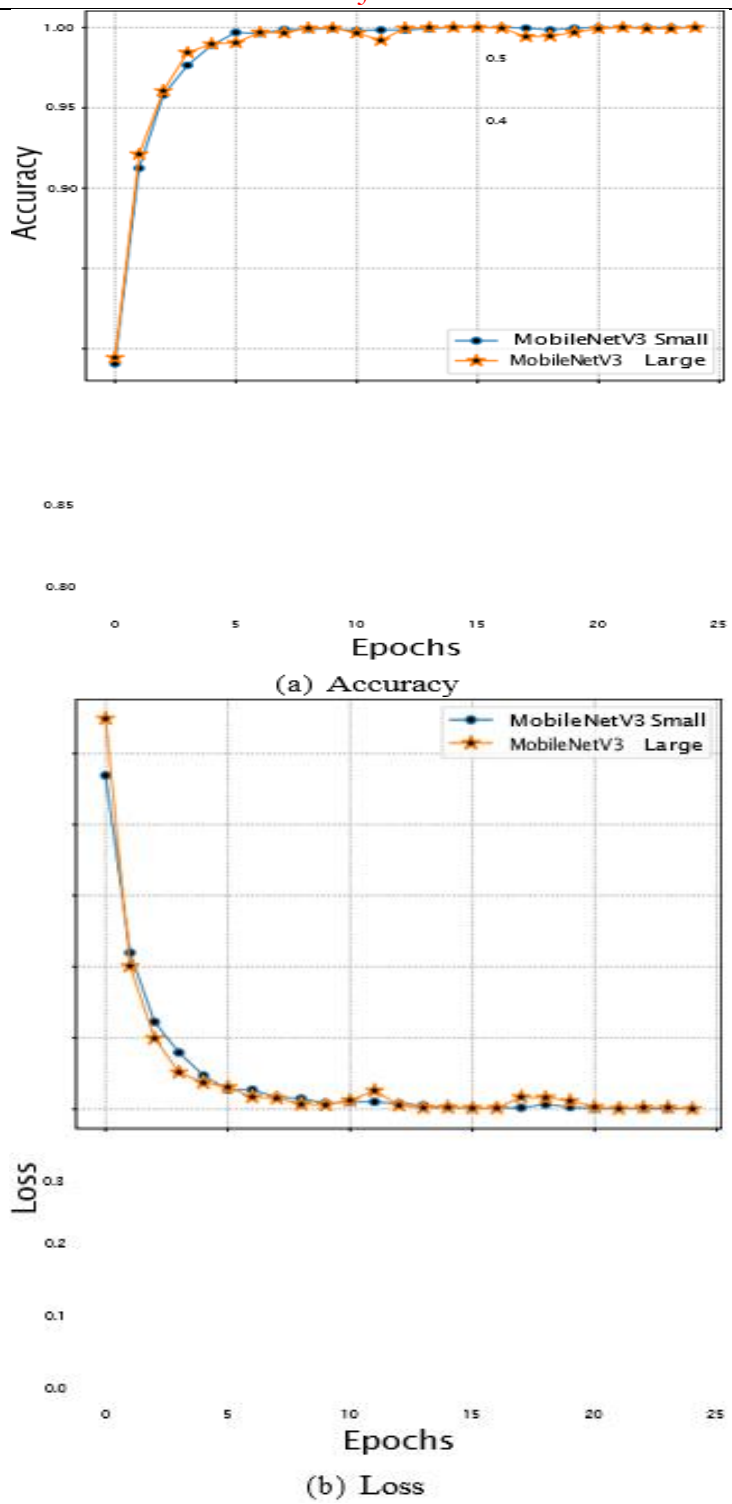


Figure 6. Accuracy and Loss Graphs with Mathematical Morphology: (a) Accuracy, (b) Loss.

References:

[1] C. Barata, M. E. Celebi, and J. S. Marques, "Improving dermoscopy image classification using color constancy," *IEEE J. Biomed. Heal. Informatics*, vol. 19, no. 3, pp. 1146–1152, May 2015, doi: 10.1109/JBHI.2014.2336473.

[2] M. K. Ilker Ali OZKAN, "Skin Lesion Classification using Machine Learning Algorithms," *Int. J. Intell. Syst. Appl. Eng.*, vol. 5, no. 4, pp. 285–289, 2017, [Online]. Available:

https://ijisae.org/index.php/IJISAE/article/view/714
[3] V. Ma and M. V. Karki, "Skin Cancer Detection using Machine Learning Techniques," *Proc. CONECCT 2020 - 6th IEEE Int. Conf. Electron. Comput. Commun. Technol.*, Jul. 2020, doi: 10.1109/CONECCT50063.2020.9198489.
[4] S. Sivaraj, R. Malmathanraj, and P. Palanisamy, "Detecting anomalous growth of skin lesion using threshold-based segmentation algorithm and Fuzzy K-Nearest Neighbor classifier," *J. Cancer Res. Ther.*, vol. 16, no. 1, pp. 40–52, Jan. 2020, doi: 10.4103/JCRT.JCRT_306_17,.
[5] Z. Waheed, A. Waheed, M. Zafar, and F. Riaz, "An efficient machine learning approach for the detection of melanoma using dermoscopic images," *Proc. 2017 Int. Conf. Commun. Comput. Digit. Syst. C-CODE 2017*, pp. 316–319, May 2017, doi: 10.1109/C-CODE.2017.7918949.
[6] S. E. F. YILMAZ, B. UZUN, "The Diagnosis of Melanoma Skin Cancer Using Histogram of Oriented Gradient based Features," in 2nd International Congress on Engineering and Arthitecture. Accessed: Apr. 26, 2025. [Online]. Available: https://www.researchgate.net/publication/344165942_The_Diagnosis_of_Melanoma_Skin_Cancer_Using_Histogram_of_Oriented_Gradient_based_Features
[7] M. P. and N. A. Praveen Banasode, "A Melanoma Skin Cancer Detection Using Machine Learning Technique: Support Vector Machine," *IOP Conf. Ser. Mater. Sci. Eng.*, vol. 1065, p. 012039, 2020, doi: 10.1088/1757-899X/1065/1/012039.
[8] V. R. Balaji, S. T. Suganthi, R. Rajadevi, V. Krishna Kumar, B. Saravana Balaji, and S. Pandiyan, "Skin disease detection and segmentation using dynamic graph cut algorithm and classification through Naive Bayes classifier," *Measurement*, vol. 163, p. 107922, Oct. 2020, doi: 10.1016/J.MEASUREMENT.2020.107922.
[9] U. O. Dorj, K. K. Lee, J. Y. Choi, and M. Lee, "The skin cancer classification using deep convolutional neural network," *Multimed. Tools Appl.*, vol. 77, no. 8, pp. 9909–9924, Apr. 2018, doi: 10.1007/S11042-018-5714-1/METRICS.
[10] S. S. Chaturvedi, K. Gupta, and P. S. Prasad, "Skin Lesion Analyser: An Efficient Seven-Way Multi-class Skin Cancer Classification Using MobileNet," *Adv. Intell. Syst. Comput.*, vol. 1141, pp. 165–176, 2021, doi: 10.1007/978-981-15-3383-9_15.
[11] K. M. Hosny, M. A. Kassem, and M. M. Foaud, "Skin Cancer Classification using Deep Learning and Transfer Learning," *2018 9th Cairo Int. Biomed. Eng. Conf. CIBEC 2018 - Proc.*, pp. 90–93, Jul. 2018, doi: 10.1109/CIBEC.2018.8641762.
[12] A. Khamparia, P. K. Singh, P. Rani, D. Samanta, A. Khanna, and B. Bhushan, "An internet of health things-driven deep learning framework for detection and classification of skin cancer using transfer learning," *Trans. Emerg. Telecommun. Technol.*, vol. 32, no. 7, p. e3963, Jul. 2021, doi: 10.1002/ETT.3963.
[13] D. N. T. Le, H. X. Le, L. T. Ngo, and H. T. Ngo, "Transfer learning with class-weighted and focal loss function for automatic skin cancer classification," Sep. 2020, Accessed: Apr. 26, 2025. [Online]. Available: https://arxiv.org/pdf/2009.05977
[14] K. M. Hosny, M. A. Kassem, and M. M. Foaud, "Classification of skin lesions using transfer learning and augmentation with Alex-net," *PLoS One*, vol. 14, no. 5, p. e0217293, May 2019, doi: 10.1371/JOURNAL.PONE.0217293.
[15] A. Mahbod, G. Schaefer, C. Wang, R. Ecker, and I. Ellinge, "Skin Lesion Classification Using Hybrid Deep Neural Networks," *ICASSP, IEEE Int. Conf. Acoust. Speech Signal Process. - Proc.*, vol. 2019-May, pp. 1229–1233, May 2019, doi: 10.1109/ICASSP.2019.8683352.
[16] and S. E. F. YILMAZ, B. UZUN, "Multiclass Skin Cancer Classification Using Ensemble of Fine-Tuned Deep Learning Models," in 2nd International Congress on Engineering and Arthitecture. Accessed: Apr. 26, 2025. [Online]. Available: https://www.researchgate.net/publication/356165036_Multiclass_Skin_Cancer_Classificati

on_Using_Ensemble_of_Fine-Tuned_Deep_Learning_Models
[17] S. Jiang, H. Li, and Z. Jin, "A Visually Interpretable Deep Learning Framework for Histopathological Image-Based Skin Cancer Diagnosis," *IEEE J. Biomed. Heal. Informatics*, vol. 25, no. 5, pp. 1483–1494, May 2021, doi: 10.1109/JBHI.2021.3052044,.
[18] B. Shetty, R. Fernandes, A. P. Rodrigues, R. Chengoden, S. Bhattacharya, and K. Lakshmanna, "Skin lesion classification of dermoscopic images using machine learning and convolutional neural network," *Sci. Rep.*, vol. 12, no. 1, pp. 1–11, Dec. 2022, doi: 10.1038/S41598-022-22644-9;SUBJMETA=114,4033,631,692,699;KWRD=COMPUTATIONAL+BIOLOGY+AND+BIOINFORMATICS,SKIN+DISEASES.
[19] K. Kaplan, Y. Kaya, M. Kuncan, and H. M. Ertunç, "Brain tumor classification using modified local binary patterns (LBP) feature extraction methods," *Med. Hypotheses*, vol. 139, p. 109696, Jun. 2020, doi: 10.1016/J.MEHY.2020.109696.
[20] N. Noreen, S. Palaniappan, A. Qayyum, I. Ahmad, M. Imran, and M. Shoaib, "A Deep Learning Model Based on Concatenation Approach for the Diagnosis of Brain Tumor," *IEEE Access*, vol. 8, pp. 55135–55144, 2020, doi: 10.1109/ACCESS.2020.2978629.
[21] M. Toğaçar, B. Ergen, and Z. Cömert, "BrainMRNet: Brain tumor detection using magnetic resonance images with a novel convolutional neural network model," *Med. Hypotheses*, vol. 134, Jan. 2020, doi: 10.1016/J.MEHY.2019.109531,.
[22] A. Esteva *et al.*, "Dermatologist-level classification of skin cancer with deep neural networks," *Nat. 2017 5427639*, vol. 542, no. 7639, pp. 115–118, Jan. 2017, doi: 10.1038/nature21056.
[23] K. Manasa and D. Murthy, "Skin cancer detection using vgg-16," *Eur. J. Mol. Clin. Med.*, vol. 8, no. 1, pp. 1419–1426, 2021.
[24] A. Howard *et al.*, "Searching for MobileNetV3," *Proc. IEEE Int. Conf. Comput. Vis.*, vol. 2019-October, pp. 1314–1324, May 2019, doi: 10.1109/ICCV.2019.00140.
[25] A. Demir, F. Yilmaz, and O. Kose, "Early detection of skin cancer using deep learning architectures: Resnet-101 and inception-v3," *TIPTEKNO 2019 - Tip Teknol. Kongresi*, vol. 2019-January, Oct. 2019, doi: 10.1109/TIPTEKNO47231.2019.8972045.
[26] S. Bechelli and J. Delhommelle, "Machine Learning and Deep Learning Algorithms for Skin Cancer Classification from Dermoscopic Images," *Bioengineering*, vol. 9, no. 3, p. 97, Mar. 2022, doi: 10.3390/BIOENGINEERING9030097.

Copyright © by authors and 50Sea. This work is licensed under Creative Commons Attribution 4.0 International License.